Neutron capture cross sections of ^{69}Ga and ^{71}Ga at 25 keV and $E_{\text{peak}} = 90$ keV

Kathrin Göbel[1,a], Clemens Beinrucker[1], Philipp Erbacher[1], Stefan Fiebiger[1], Micaela Fonseca[1,2,3], Michael Heftrich[1], Tanja Heftrich[1], Franz Käppeler[4], Antonin Krása[5], Claudia Lederer-Woods[1,6], Ralf Plag[1,7], Arjan Plompen[8], René Reifarth[1], Stefan Schmidt[1], Kerstin Sonnabend[1], and Mario Weigand[1]

[1] Goethe University Frankfurt, Germany
[2] LIBPhys-UNL, DF, FCT, Universidade Nova de Lisboa, Portugal
[3] Universidade Europeia, Laureate International Universities, Portugal
[4] Karlsruher Institut für Technologie, Germany
[5] SCK-CEN, Belgian Nuclear Research Centre, Mol, Belgium
[6] University of Edinburgh, UK
[7] GSI Helmholtzzentrum für Schwerionenforschung, Darmstadt, Germany
[8] Joint Research Centre (EC-JRC), Geel, Belgium

Abstract. We measured the neutron capture cross sections of ^{69}Ga and ^{71}Ga for a quasi-stellar spectrum at $k_{\text{B}}T = 25$ keV and a spectrum with a peak energy at 90 keV by the activation technique at the Joint Research Centre (JRC) in Geel, Belgium. Protons were provided by an electrostatic Van de Graaff accelerator to produce neutrons via the reaction ^{7}Li(p,n). The produced activity was measured via the γ emission of the product nuclei by high-purity germanium detectors. We present preliminary results.

1. Introduction

Most of the elements heavier than iron are produced by the slow (s) and the rapid (r) neutron capture processes. The s-process takes place during stellar He and C burning phases with neutron densities between 10^8 and 10^{10} cm^{-3}. The reaction path closely follows the valley of stability since neutron capture times of typically one to ten years are much slower than most of the β-decay times of the involved nuclei [1].

The s-process is composed of the weak and the main component [2]. The main differences lie in the neutron-to-seed ratios, the temperatures as well as the neutron densities. The main component of the s-process takes place at about 5 to 25 keV in low-mass asymptotic giant branch (AGB) stars and produces the nuclei with mass numbers above $A \approx 90$ [2]. The weak component of the s-process takes place in massive stars of more than eight solar masses during convective helium burning at temperatures of about 30 keV and during convective shell carbon burning at about 90 keV. The time-integrated neutron flux is lower compared to the main component producing nuclei with mass numbers $A \leq 90$.

2. The weak s-process

The weak s-process produces most of the s-process isotopes between iron and strontium. The neutron fluence in the weak s-process is too low to achieve reaction flow equilibrium, in contrast to the main s-process component. Therefore, a particular neutron capture cross section not only determines the abundance of the respective isotope (as in the case of the main component), but affects the abundances of all heavier isotopes as well.

The uncertainties of the neutron capture cross sections of the weak s-process nuclei ($60 \leq A \leq 90$) are higher than the uncertainties of the main s-process nuclei ($A \geq 90$). Following the weak s-process path, the cumulated uncertainties affect all isotopes of the weak s-process, up to krypton and strontium, with possible minor contributions to the yttrium and zirconium abundances [1,3,4]. Accurate predictions require the cross sections to be known with an accuracy of at least 5% for all involved nuclei in the weak s-process [5].

3. The case of gallium

Gallium is mostly produced by the weak s-process in massive stars. Recent simulations [3] show that gallium is the most abundant s-element at the end of shell carbon burning. So far, there is only a time-of-flight measurement with a sample of natural gallium [6]. Other nuclei (^{81}Br, ^{75}As, ^{74}Ge) measured within the same experimental campaign show large deviations from more recent results [7]. For ^{71}Ga two discrepant results from integral measurements at 25 keV are published [8,9]. The cross sections should be remeasured to solve the discrepancies. Data for carbon shell burning in massive stars at 90 keV are highly desired.

[a] e-mail: goebel@physik.uni-frankfurt.de

Table 1. Parameters for the simulation of the neutron spectra with PINO [11].

Proton energy	Peak energy of neutron spectrum	Lithium target		Ga activation sample	
		Thickness	Radius	Distance to Lithium	Radius
(1912 ± 2) keV	25 keV	27.5 μm	3 mm	1.0 mm	6 mm
(1920 ± 2) keV	90 keV	1.15 μm	3 mm	9.7 mm	6 mm
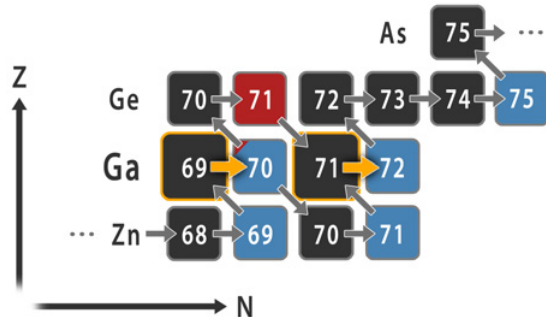
Figure 1. Path of the s-process between zinc and arsenic. The neutron capture cross sections were measured at 25 keV and 90 keV by activation for the isotopes ^{69}Ga and ^{71}Ga, which are marked in yellow.
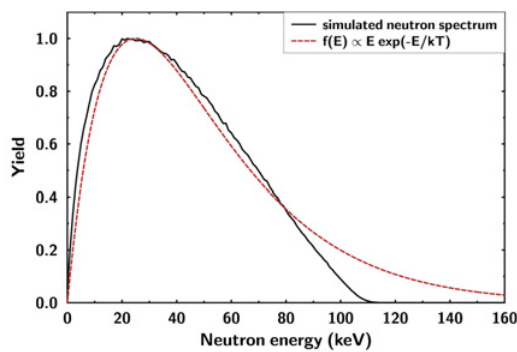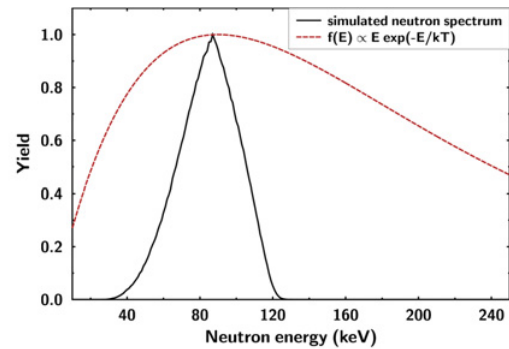

Figure 2. Simulated neutron spectrum with a peak energy at 25 keV [11]. The parameters for the simulation are given in Table 1. The red dashed line shows the corresponding Maxwell-Boltzmann distribution for $k_\mathrm{B}T = 25$ keV.

4. Activation

The activation was carried out at the Joint Research Centre (JRC) in Geel, Belgium. An electrostatic Van de Graaff accelerated protons to the necessary energy to produce neutrons via the reaction ^{7}Li(p,n). The neutron flux was monitored by a B$_4$F ionisation chamber. Samples of natural gallium positioned between two gold monitors were irradiated with neutrons with two different energy spectra: (a) a quasi-stellar spectrum with $k_\mathrm{B}T = 25$ keV and (b) a spectrum with a peak energy at 90 keV [10]. The beam parameters and the properties of the lithium and the gallium samples are given in Table 1. The neutron spectra were simulated with PINO [11] and are shown in Figs. 2 and 3.

5. Analysis

The produced activity was determined by γ-ray spectroscopy with high-purity germanium detectors. In the case of ^{69}Ga we used the γ lines with energies of 176 keV and 1039 keV from the decay of ^{70}Ga, in the case of ^{71}Ga we used the γ lines 601 keV, 629 keV, 835 keV,

Figure 3. Simulated neutron spectrum with a peak energy at 90 keV [11]. The parameters for the simulation are given in Table 1. The red dashed line shows the corresponding Maxwell-Boltzmann distribution for $k_\mathrm{B}T = 90$ keV.

894 keV and 1051 keV from the decay of ^{72}Ga. Higher-energy γ lines were not considered since the efficiency was only determined up to about 1330 keV using a calibration source.

The cross section is calculated by

$$\sigma = \frac{N_\mathrm{produced}}{\Phi_\mathrm{n} \cdot N_\mathrm{sample}} \qquad (1)$$

where N_produced is the number of produced nuclei, Φ_n is the integrated neutron flux, and N_sample is the number of sample nuclei.

The number of sample nuclei was determined by the sample mass. The number of produced nuclei is calculated from the counts in the γ line with several correction factors:

$$N_\mathrm{produced} = \frac{C}{I_\gamma \cdot \epsilon \cdot \kappa \cdot f_\mathrm{dt} \cdot f_\mathrm{b} \cdot f_\mathrm{dw} \cdot f_\mathrm{casc}} \qquad (2)$$

where C is the number of counts for one γ line, I_γ is the corresponding γ intensity, and κ is the self-absorption. The factor f_dt corrects for the deadtime, f_b for the decays during the activation, f_dw for the decays before and after the measurement, and f_casc for the decay cascades.

6. Preliminary results

The analysis of the activation experiment gives the ratio of the neutron capture cross sections of ^{69}Ga and ^{197}Au as well as of ^{71}Ga and ^{197}Au. The results are shown in Table 2. The neutron capture cross sections at $k_\mathrm{B}T = 25$ keV can be calculated from the ratios using the MACS of ^{197}Au(n,γ) at 25 keV (683 mb), which was taken from Ref. [12]. Table 3 compares the results to the MACSs from KADoNiS v0.3 [7], which were renormalized with the ^{197}Au cross section value from Ref. [12]. The measured value for ^{69}Ga is about 30% higher than the evaluated value, the measured value for ^{71}Ga is about 20% lower.

Table 2. Ratios of neutron capture cross sections for $k_B T = 25\,\text{keV}$ and for the neutron spectrum with $E_{\text{peak}} = 90\,\text{keV}$.

	Neutron spectrum for	
	25 keV	90 keV
$\sigma_{69\text{Ga}}/\sigma_{197\text{Au}}$	0.31	0.29
$\sigma_{71\text{Ga}}/\sigma_{197\text{Au}}$	0.18	0.17

Table 3. Neutron capture cross sections at $k_B T = 25\,\text{keV}$. The $^{197}\text{Au}(n,\gamma)$ MACS at 25 keV (683 mb) was taken from Ref. [12]. The MACS from KADoNiS v0.3 was renormalized with this value.

	σ	MACS
	measured	KADoNiS v0.3 [7, 12]
^{69}Ga	212 mb	161 mb
^{71}Ga	123 mb	145 mb

References

[1] R. Reifarth, C. Lederer, F. Käppeler, Journal of Physics G Nuclear Physics **41**(5), 053101 (2014)

[2] P.A. Seeger, W.A. Fowler, D.D. Clayton, The Astrophysical Journal, Supplement **11**, 121 (1965)

[3] M. Pignatari, R. Gallino, M. Heil, M. Wiescher, F. Käppeler, F. Herwig, S. Bisterzo, The Astrophysical Journal **710**, 1557 (2010)

[4] M. Weigand, T.A. Bredeweg, A. Couture, K. Göbel, T. Heftrich, M. Jandel, F. Käppeler, C. Lederer, N. Kivel, G. Korschinek et al., Physical Review C **92**(4), 045810 (2015)

[5] Z.Y. Bao, H. Beer, F. Käppeler, F. Voss, K. Wisshak, T. Rauscher, Atomic Data and Nuclear Data Tables **76**, 70 (2000)

[6] G. Walter, KfK Bericht **3706** (1984)

[7] I. Dillmann, R. Plag, F. Käppeler, T. Rauscher, Proceedings of the workshop "'EFNUDAT Fast Neutrons - scientific workshop on neutron measurements, theory & applications"', Geel, Belgium (2009)

[8] R. Anand, M. Jhingan, D. Bhattacharya, E. Kondaiah, Nuovo Cimento **50A**, 247 (1979)

[9] G. Walter, H. Beer, F. Käppeler, G. Reffo, F. Fabbri, Astronomy and Astrophysics **167**, 186 (1986)

[10] R. Reifarth, M. Heil, C. Forssén, U. Besserer, A. Couture, S. Dababneh, L. Dörr, J. Görres, R.C. Haight, F. Käppeler et al., Physical Review C **77**(1), 015804 (2008)

[11] R. Reifarth, M. Heil, F. Käppeler, R. Plag, Nuclear Instruments and Methods in Physics Research A **608**, 139 (2009)

[12] C. Massimi, B. Becker, E. Dupont, S. Kopecky, C. Lampoudis, R. Massarczyk, M. Moxon, V. Pronyaev, P. Schillebeeckx, I. Sirakov et al., European Physical Journal A **50**, 124 (2014)